Boundary-Layer Meteorol (2009) 130:407–422
DOI 10.1007/s10546-009-9350-1

ORIGINAL PAPER

Low-Level Wind Forecast over the La Plata River Region with a Mesoscale Boundary-Layer Model Forced by Regional Operational Forecasts

L. Sraibman · G. J. Berri

Received: 4 March 2008 / Accepted: 5 January 2009 / Published online: 22 January 2009

Abstract A mesoscale boundary-layer model (BLM) is used for running 12-h low-level wind forecasts for the La Plata River region. Several experiments are performed with different boundary conditions that include operational forecasts of the Eta/CPTEC model, local observations, as well as a combination of both. The BLM wind forecasts are compared to the surface wind observations of five weather stations during the period November 2003–April 2004. Two accuracy measures are used: the hit rate or percentage of cases with agreement in the wind direction sector, and the root-mean-squared error (RMSE) of the horizontal wind components. The BLM surface wind forecasts are always more accurate, since its averaged hit rate is three times greater and its averaged RMSE is one half smaller than the Eta forecasts. Despite the large errors in the surface winds displayed by the Eta forecasts, its 850 hPa winds and surface temperature forecasts are able to drive the BLM model to obtain surface winds forecasts with smaller errors than the Eta model. An additional experiment demonstrates that the advantage of using the BLM model for forecasting low-level winds over the La Plata River region is the result of a more appropriate definition of the land–river surface temperature contrast. The particular formulation that the BLM model has for the geometry of the river coasts is fundamental for resolving the smaller scale details of the low-level local circulation. The main conclusion of the study is that operational low-level wind forecasts for the La Plata River region can be improved by running the BLM model forced by the Eta operational forecasts.

Keywords Boundary-layer model · Low-level wind forecast · Model coupling

L. Sraibman and G. J. Berri—Members of Consejo Nacional de Investigaciones Científicas y Técnicas (CONICET) of Argentina.

L. Sraibman (✉) · G. J. Berri
Departamento de Ciencias de la Atmósfera y los Océanos, Facultad de Ciencias Exactas y Naturales, Universidad de Buenos Aires, Buenos Aires, Argentina
e-mail: laurasra@at.fcen.uba.ar

G. J. Berri
e-mail: berri@at.fcen.uba.ar

Fig. 1 Geographical location of the La Plata River and mean observed wind roses for the period November 2003–April 2004 at the meteorological stations Aeroparque, Don Torcuato, Ezeiza, Colonia and Carrasco. The scale in the lower left corner indicates the wind direction frequency as a percentage

1 Introduction

The La Plata River is 300 km long and between 40 and 200 km wide, and flows into the Atlantic Ocean in central-eastern South America (see Fig. 1). This extended water surface is a conditioning and regulating factor of the local weather and climate that influences air pollution, tide regime, fishing, harbour operations, tourism, etc. The La Plata River region is of significant importance to Argentina and Uruguay since some of their most industrialized and populated cities are located in the area. Due to the extension and the geography of the La Plata River shores, a local atmospheric circulation develops in the lower levels, with the cyclic characteristics of the sea–land breeze circulation. This circulation is generated by the temperature difference between land and river and the wind blows from water to land during the day (i.e., sea breeze), while at night flow is from land to water (i.e., land breeze). Since this is a flat terrain region there are no other topographical effects that influence the low-level local circulation.

Several numerical models have been used to study sea–land breeze circulations, for example Pielke (1974); Pielke et al. (1992) and Black (1994). In some regions where the sea-breeze circulation is important, it is common to adapt existent numerical models to study this local circulation. Sea-breeze cases over north-western Hawaii were simulated using the NCEP (National Center for Environmental Prediction) mesoscale spectral model coupled with an advanced land-surface model with 3-km horizontal resolution (Zhang et al. 2005). The inland penetration of the lake breeze on the western shore of Lake Michigan was studied by Roebber and Gehring (2000) using the MM5 mesoscale model with 5-km grid spacing. Some boundary-layer forecast models have been developed to study the sea-land breeze in complex terrains, for example Daggupaty (2001) for simulation of the three-dimensional circulation associated with lake breezes in south-western Ontario. One of the main problems with regional models is the resolution required to represent the short to mid–term regional–scale processes, as discussed by Colby (2004). An important aspect in modelling local circulations

is the verification of predictions, as done for example by Case et al. (2004) over east central Florida.

The sea–land breeze circulation over the La Plata River region was studied by Berri and Nuñez (1993) with a mesoscale boundary-layer model (BLM) especially formulated for the area. They present a case study of a favourable synoptic situation for the development of the sea–land breeze, showing that the BLM model is able to reproduce the observed mean wind direction changes across the region during the day. Based on that result, the objective of the present study is to adapt the BLM model (briefly described in Sect. 2), to produce diurnal operational low-level wind forecasts over the La Plata River region, with higher temporal and spatial resolution than the presently available one. As will be described in the following sections, the BLM model requires a prescribed upper and lower boundary conditions in order to produce a forecast. In the present study three experiments are performed (described in Sect. 3) with different boundary conditions, and the results are verified with local observations. In Experiment I, the BLM model is forced at the upper and lower boundaries with the forecasts of the Eta model (Mesinger and Black 1992), performed by CPTEC (Centro de Previsao de Tempo e Estudos Climáticos, Brazil). In Experiment II, the BLM model is forced at the upper boundary with the Eta model forecasts and at the lower boundary with observed surface temperatures. Experiment III employs only observations for defining the upper boundary condition (radiosonde data), and the lower boundary condition (surface temperature). In each experiment the BLM wind forecasts are compared to the available observational data and to the Eta model wind forecasts, and Sect. 4 presents the discussion and the conclusions of the study.

2 Model Description

The horizontal domain of the BLM forecasts extends over a region of approximately 430 km × 350 km and consists of 43 × 35 grid points spaced every 0.1 degrees (see Fig. 1 for geographical reference). The vertical domain has 12 levels distributed in a log–linear spacing. The first level is the roughness length z_0 (equal to 0.01 m over water and 0.10 m over land), and the last one is the material top of the model at 2,000 m. The intermediate levels are located at the following heights, 10, 40, 80, 140, 220, 350, 550, 800, 1,100 and 1,500 m.

The BLM model has been developed by Berri and Nuñez (1993), and the equations are based on the three principles that govern the atmospheric motion, i.e. conservation of momentum, mass and energy. Since the model is formulated for studying the atmospheric circulation in the boundary layer, the vertical component of the equation of motion becomes the hydrostatic equation and the mass conservation principle is approximated by the continuity equation for an incompressible fluid. The model is dry and all energy sources have been neglected, except the surface heating, so that the energy equation reduces to the conservation of potential temperature. The BLM model equations are:

$$\frac{\partial u}{\partial t} = -u\frac{\partial u}{\partial x} - v\frac{\partial u}{\partial y} - w\frac{\partial u}{\partial z} - \alpha_0\frac{\partial p}{\partial x} + fv + \frac{\partial}{\partial x}\left(K_{mh}\frac{\partial u}{\partial x}\right) + \frac{\partial}{\partial y}\left(K_{mh}\frac{\partial u}{\partial y}\right) + \frac{\partial}{\partial z}\left(K_{mz}\frac{\partial u}{\partial z}\right), \quad (1)$$

$$\frac{\partial v}{\partial t} = -u\frac{\partial v}{\partial x} - v\frac{\partial v}{\partial y} - w\frac{\partial v}{\partial z} - \alpha_0\frac{\partial p}{\partial y} - fu$$

$$+\frac{\partial}{\partial x}\left(K_{mh}\frac{\partial v}{\partial x}\right)+\frac{\partial}{\partial y}\left(K_{mh}\frac{\partial v}{\partial y}\right)+\frac{\partial}{\partial z}\left(K_{mz}\frac{\partial v}{\partial z}\right), \tag{2}$$

$$\frac{\partial\theta}{\partial t}=-u\frac{\partial\theta}{\partial x}-v\frac{\partial\theta}{\partial y}-w\frac{\partial\theta}{\partial z}+\frac{\partial}{\partial x}\left(K_{\theta h}\frac{\partial\theta}{\partial x}\right)+\frac{\partial}{\partial y}\left(K_{\theta h}\frac{\partial\theta}{\partial y}\right)+\frac{\partial}{\partial z}\left(K_{\theta z}\frac{\partial\theta}{\partial z}\right), \tag{3}$$

$$\frac{\partial w}{\partial z}=-\frac{\partial u}{\partial x}-\frac{\partial v}{\partial y}, \tag{4}$$

$$\frac{\partial p_0}{\partial z}=-\frac{g}{\alpha_0}, \tag{5}$$

$$\frac{\partial p'}{\partial z}=\frac{g}{\alpha_0}\frac{\theta'}{\theta_0}, \tag{6}$$

$$p=p_0+p', \tag{7}$$

$$\theta'=\theta-\theta_0, \tag{8}$$

where all symbols have the usual meteorological meaning, subscript 0 refers to a horizontally-averaged value over the entire domain, and the prime refers to a local departure from that average value. Equations 1–3 are the forecast equations for the u and v wind components and potential temperature θ, respectively. Equations 4–8 are the diagnostic equations for the vertical motion w, atmospheric pressure p_0, p' and p, and potential temperature departure θ', respectively. Equations 1–8 are solved from the top of the surface layer ($z = 40$ m) to the material top of the model by a semi–implicit numerical scheme. Within the constant-flux layer, the forecast equations become diagnostic equations by applying the similarity theory, and therefore reduce to logarithmic vertical profiles of wind and potential temperature, as a function of stability. The boundary conditions at the top of the model are: $u = u_g$, $v = v_g$, $w = p' = \theta' = 0$, where u_g and v_g are the geostrophic wind components. At the lower boundary the conditions are: $u = v = w = 0$, whereas θ is defined at every timestep (see Subsect. 3.2.2 below). At the lateral boundaries, all variables are allowed to change in order to provide a zero gradient across the boundaries at each timestep. The model is initialized under conditions of horizontal homogeneity for all the variables, except p and p_0, since their gradients define geostrophic wind at the initial state. Thus, Eq. 5 is integrated once and Eqs. 1 and 2, which become the well-known Ekman layer equations, are integrated during three inertial periods in order to remove any possible inertial oscillations from the solution. For more details about the model formulation and the numerical method of solution, see Berri and Nuñez (1993).

3 Experiment Design

A set of three experiments is performed, each one consisting of 142 diurnal forecasts obtained with the BLM model during the summer period from November 2003 to April 2004. The number of cases is less than the 182 days of that period, since the set of forecasts is restricted to those days with complete hourly observations. Each set member is a 12-h forecast starting at 0900 local standard time (LST), approximately 2–3 h after sunrise, when there is a minimum land–river temperature contrast. In this first study of BLM operational forecast

verification, the forecast horizon is limited to the diurnal cycle, since the results of Berri and Nuñez (1993) show that the most remarkable changes in the wind pattern take place during the daytime hours. The forecast wind is compared to the observed wind at the following five weather stations: Aeroparque, Don Torcuato and Ezeiza in Argentina, and Colonia and Carrasco in Uruguay (see Fig. 1 for their location). The 0900 LST BLM forecast is taken after 30 min of model integration, in order to facilitate the model spin-up. Figure 1 shows the observed mean wind direction frequencies at the five weather stations during November 2003–April 2004. The figure shows significant differences in the predominant wind direction sectors across the La Plata River region, as a consequence of the dominant sea–land breeze circulation.

3.1 Evaluation Method

The BLM and Eta model 10-m wind forecasts are validated with observations at the weather stations, by means of two accuracy measures. One is the hit rate (HR) that counts the percentage of cases that the forecast wind direction matches the observed wind direction (Wilks 1995), and the other one is the root-mean-squared error (RMSE) of the horizontal wind components. In order to calculate the HR, the horizontal wind components are transformed to a wind direction expressed as one of the eight standard compass sectors (north, north-east, east, etc.). The RMSE is a usual accuracy measure employed in forecast verification (for example Hanna and Yang 2001; White et al. 1999; Zhong and Fast 2003), and is calculated as

$$RMSE = \sqrt{\frac{1}{N}\left(\sum_{j=1}^{N}(u_o - u_f)_j^2 + \sum_{j=1}^{N}(v_o - v_f)_j^2\right)}, \tag{9}$$

where N is the number of available observations, u and v are the zonal and meridional wind components, respectively, subscripts f and o refer to forecast and observation, respectively, and subscript j identifies the observation to be verified. The BLM forecasts are verified with each available observation between 0900 and 2100 LST, while the Eta forecasts are verified with the 0900, 1500 and 2100 LST observations, since these are the only model outputs available for the study. Since the terrain is flat, the verification of both models is made with the interpolated value of the four surrounding grid points to each weather station (the interpolation uses the same technique that is described in Sect. 3.2.1).

3.2 Experiment I

In this set of forecasts the BLM is forced at the upper and lower boundaries with the Eta forecasts; the Eta model produces twice daily forecasts initialized at 1200 UTC and 0000 UTC (corresponding to 0900 LST and 2100 LST, respectively). In the present study we use the 1200 UTC forecast of the previous day, since, according to Mesinger and Black (1992), Seluchi and Chou (2001) and Bustamante et al. (1999), the Eta forecasts for the second 24 h are better than for the first 24 h. Thus, the BLM is initialized at 0900 LST with a 24-h Eta forecast. Since the Eta forecasts are available at 6-h intervals (i.e. 1200 UTC, 1800 UTC and 0000 UTC), it is necessary to interpolate the data in time in order to define the boundary conditions at the 1-min BLM timestep. For this purpose a cubic spline interpolating polynomial (Cormier and Marsh 2001) is implemented, which has the property of being continuous and having first-order and second-order continuous derivatives. Additionally, it is necessary to

interpolate the data in space from the 40-km resolution of the Eta model to the 10-km BLM resolution, with the technique described in the following subsection.

3.2.1 Upper Boundary Interpolation

The 850-hPa Eta wind forecasts are interpolated using the Cressman method (Cressman 1959); the first step consists of calculating the distance D_{ij}^k from each BLM grid point, identified by subscripts i and j, to every Eta grid point, identified with the superscript k. This distance is given by $D_{ij}^{k2} = (X_k - X_{ij})^2 + (Y_k - Y_{ij})^2$, where X_{ij} and Y_{ij} are the longitude and latitude, respectively, of the BLM grid points, and X_k and Y_k are the longitude and latitude, respectively, of the Eta grid points. The second step consists of calculating the weighting factor of each grid point as follows: $W_{ij}^k = (N^2 - D_{ij}^{k2})/(N^2 + D_{ij}^{k2})$, if $N \geq D_{ij}^k$, and $W_{ij}^k = 0$, if $N < D_{ij}^k$, where N is a fixed value that, after testing the results of the interpolation, was set equal to 0.4 degrees. Finally, the corresponding value of any variable at each BLM grid point is given by $V_{ij} = \sum_k V^k W_{ij}^k / \sum_k W_{ij}^k$, where V^k is the corresponding value at the Eta grid point.

3.2.2 Lower Boundary Interpolation

A similar interpolating routine is implemented at the lower boundary, although it is applied separately to the grid points over the land and over the river. The reason for this procedure is because the temperature over the river is quite homogeneous and changes very little during the day, whereas over land the daily cycle of temperature is large, with an amplitude that can exceed 10°C. Therefore, a 1-km transition band centred at the coast is established, in which the land–river surface temperature difference is linearly interpolated. This provides a smooth transition between the two regions and concentrates the land–river temperature contrast at the coast.

3.2.3 Results of Experiment I

Table 1 shows that the BLM RMSE is between 2.4 and 3.3 m s^{-1} smaller than the Eta RMSE, while the BLM HR value is almost three times greater than the corresponding Eta HR, in all cases. Figure 2 compares the HR obtained with both models at every weather station, at three different times of the day, as well as its average value. At all weather stations the BLM wind direction forecasts are more accurate than the Eta wind direction forecasts, with the greatest

Table 1 HR and RMSE for experiment I

	0900 LST		1500 LST		2100 LST		Average 0900, 1500 and 2100 LST		Average from 0900 to 2100 LST	
	HR (%)	RMSE (m s^{-1})	HR (%)	RMSE (m s^{-1})	HR (%)	RMSE (m s^{-1})	HR (%)	RMSE (m s^{-1})	HR (%)	RMSE (m s^{-1})
BLM	68	3.2	50	3.5	58	3.6	59	3.4	58	3.5
Eta	21	5.6	18	6.8	15	6.5	18	6.4		

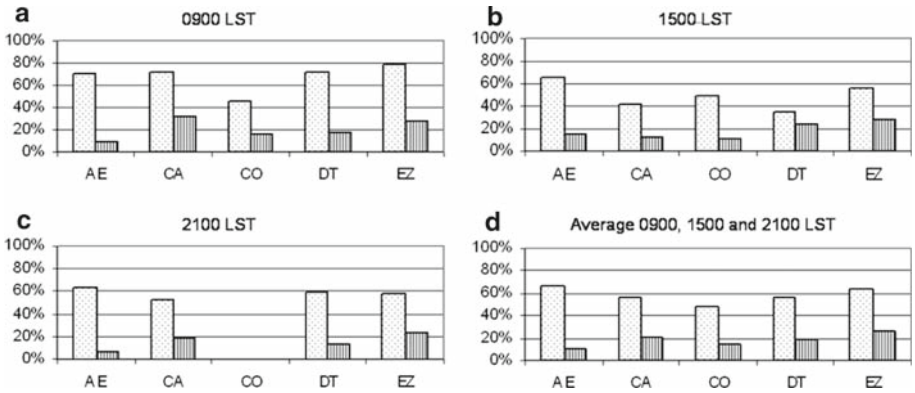

Fig. 2 HR rates for Experiment I at **a** 0900 LST, **b** 1500 LST, **c** 2100 LST and **d** average of 0900, 1500 and 2100 LST, for the meteorological stations Aeroparque (AE), Carrasco (CA), Colonia (CO), Don Torcuato (DT) and Ezeiza (EZ). The *dotted* (*dashed*) bar corresponds to the BLM (Eta) model

HR values at 0900 LST. The improvement of the BLM forecasts over the Eta forecasts is more significant at Aeroparque, the closest weather station to the river shore.

The analysis of the BLM wind field forecast (not shown) revealed an excessive predominance of the inland wind component at 1500 LST, suggesting a stronger than normal sea breeze. The BLM surface forcing is the land–river temperature difference, so that the larger the thermal contrast the stronger the sea–land breeze circulation.

In order to compare the magnitude of the Eta model thermal contrast with the observations, we calculated the temperature difference between Ezeiza (inland) and Pontón Recalada (river). We chose Ezeiza as the most representative inland weather station, located several kilometres away from the coast, while Pontón Recalada is the only weather station over the river (see Fig. 1). The observed temperature difference is compared to the temperature difference calculated between the nearest Eta grid points to Ezeiza and Pontón Recalada.

The mean observed temperature differences are 1, 4 and 1°C, at 0900, 1500 and 2100 LST, respectively, whereas the corresponding Eta values are 1, 10 and −2°C, respectively. The greatest departure of the Eta land–river thermal contrast from the observations takes place in the afternoon, which is the cause of the stronger than normal sea-breeze component of the BLM forecasts. In an attempt to improve the BLM results, a new experiment is designed in which the surface forcing is defined from the observations.

3.3 Experiment II

In this case the BLM model is forced by a surface potential temperature given by the expression: $\theta(x, y, t) = \theta_0 + A(t)[1 + \tanh(s(x, y)/B)]$, where θ_0 is the mean value of the surface potential temperature over the entire domain at the initial state. The land–river temperature difference, $A(t)$, is calculated as the harmonic analysis of the observed temperature differences between Ezeiza and Pontón Recalada at 0300, 0900, 1500 and 2100 LST. Finally, $s(x, y)$ is the shortest distance between every grid point and the coast, where the hyperbolic tangent distributes the land–river temperature difference symmetrically with respect to the coast. The parameter B, set equal to 1,000 m, accounts for 75% (90%) of the temperature change in a distance equal to $2B$ ($3B$) across the coast. The upper boundary condition of the BLM model is the same as Experiment I.

Table 2 HR and RMSE for experiment II

	0900 LST		1500 LST		2100 LST		Average 0900, 1500 and 2100 LST		Average from 0900 to 2100 LST	
	HR (%)	RMSE ($m\,s^{-1}$)	HR (%)	RMSE ($m\,s^{-1}$)	HR (%)	RMSE ($m\,s^{-1}$)	HR (%)	RMSE ($m\,s^{-1}$)	HR (%)	RMSE ($m\,s^{-1}$)
BLM	64	3.7	60	4.2	45	3.7	56	3.8	58	4.3
Eta	21	5.6	18	6.8	15	6.5	18	6.4		

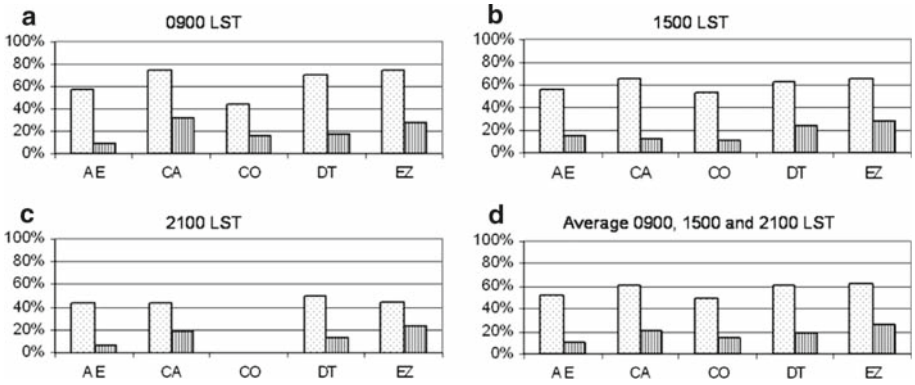

Fig. 3 Same as Fig. 2, but for Experiment II

3.3.1 Results of Experiment II

Table 2 compares the RMSE and HR values of both models, and again the BLM forecasts are more accurate than the Eta forecasts, although the average values compare less well than in Experiment I. For example, the 56% average HR is slightly smaller than the 59% average HR of Experiment I (see column 4), and the average 3.8 m s^{-1} RMSE is slightly greater than the 3.4 m s^{-1} RMSE of Experiment I. It is interesting, however, to analyse the results at different times of the day. For example, at 1500 LST the 60% HR represents a significant improvement over the 50% HR of Experiment I, although the 4.2 m s^{-1} RMSE is greater than the 3.5 m s^{-1} RMSE of Experiment I. On the other hand, the BLM forecasts at 0900 and 2100 LST are less accurate in comparison to Experiment I. For example the HR value drops from 68 to 64% at 0900 LST and from 58 to 45% at 2100 LST. Similarly, the RMSE increases from 3.2 to 3.7 m s^{-1} at 0900 LST and from 3.6 to 3.7 m s^{-1} at 2100 LST. The improvement of the BLM afternoon forecasts is the result of a more appropriate definition of the land–river thermal contrast, since the excessive forcing provided by the Eta forecast leads to a much stronger inland sea-breeze component.

The last column of Tables 1 and 2 presents the averaged BLM HR and RMSE for all the hours between 0900 LST and 2100 LST. In this case, Experiment I shows a minor improvement over Experiment II in the case of the RMSE, but not for HR, which remains the same. Clearly, a better definition of the surface forcing improves the BLM forecasts at 1500 LST. Figure 3 shows the HR value at each weather station and time of the day. It can be clearly seen at 1500 LST (Fig. 3b) that, with the only exception of Ezeiza, Experiment II forecasts are more accurate than Experiment I forecasts.

3.4 Experiment III, Model Forced with Observations

In this case, both the upper and lower boundary conditions for the BLM forecasts are defined exclusively from local observations. The surface forcing condition is the same as in Experiment II, but the upper boundary condition is taken from the 1200 UTC (0900 LST) 850-hPa level Ezeiza radiosonde sounding. Since there is only one sounding a day, the upper boundary condition remains constant during the integration period.

3.4.1 Results of Experiment III

Table 3 compares the averaged 0900, 1500 and 2100 LST RMSE and HR values at the five weather stations, obtained with the BLM forecasts performed for different boundary conditions. In the first two columns the boundary conditions are from the Eta forecasts, whereas in the following three columns the boundary conditions are from the observations. The last column shows the averaged RMSE and HR values of the Eta forecasts. In all cases the BLM forecasts are more accurate than the Eta forecasts, although there are remarkable differences among them.

When the upper boundary condition is taken from the 850-hPa radiosonde sounding (same level of the Eta forecasts as used in the previous cases), the BLM forecasts degrade with respect to Experiment I. The RMSE increases from 3.4 to 3.8 m s^{-1} and the HR drops from 59 to 41% (Table 3, columns 1 and 3). In view of this, we decided to run the BLM forecasts using other levels of the radiosonde sounding for defining the upper boundary condition. The other two standard levels available from the observations are 925 and 1,000 hPa, and the results are shown in columns 4 and 5 of Table 3. It can be seen that the forecast performance improves as the level of the boundary condition approaches surface. The best result is obtained with the 1,000-hPa level, with a 5% improvement in the HR (from 59 to 64%, Table 3, columns 1 and 5), with respect to the case in which both boundary conditions are defined from the Eta forecasts. The La Plata River region is under the influence of the South Atlantic anticyclone whose temperature inversion defines the top of the boundary layer. The analysis of the Ezeiza radiosonde data shows that in 72% of the observations during the validation period, the base of the temperature inversion is below 850 hPa, and in 54% of the cases it is below 925 hPa. Since most of the time these two levels are above the top of the boundary layer, 1,000 hPa seems to be the most appropriate standard level for defining the upper boundary condition for the BLM forecasts.

Table 3 Averaged 0900, 1500 and 2100 LST RMSE and HR values at the five meteorological stations, obtained with the Eta and the BLM models forecasts under different boundary conditions

	BLM boundary conditions from Eta forecasts		BLM boundary conditions from observations			Eta
U. bound.	850 hPa Exp I	1,000 hPa	850 hPa	925 hPa	1,000 hPa Exp III	
L. bound.	Eta temp.	Eta temp.	Temp. function	Temp. function	Temp. function	
RMSE (m s^{-1})	3.4	3.4	3.8	3.4	3.4	6.4
HR (%)	59	53	41	48	64	18

U. bound and L. bound means upper boundary and lower boundary, respectively. *Eta temp.* means that the interpolation from Eta temperature is used, and *temp. function* means that the surface potential temperature function is used

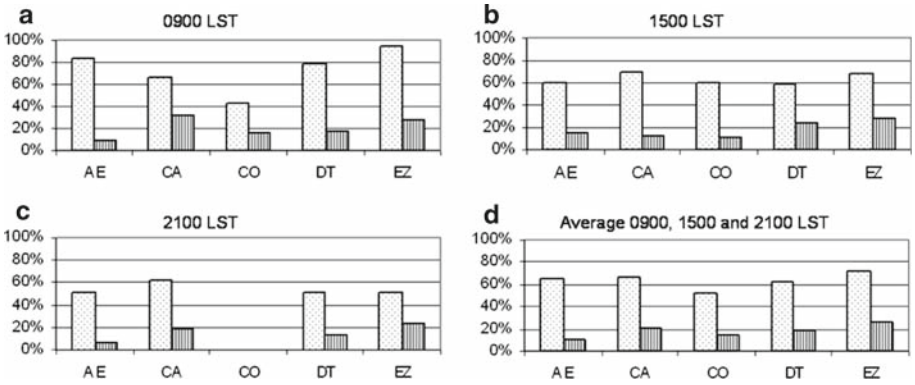

Fig. 4 Same as Fig. 2, but for Experiment III

Table 4 HR and RMSE for experiment III

	0900 LST		1500 LST		2100 LST		Average 0900, 1500 and 2100 LST		Average from 0900 to 2100 LST	
	HR (%)	RMSE (m s^{-1})	HR (%)	RMSE (m s^{-1})	HR (%)	RMSE (m s^{-1})	HR (%)	RMSE (m s^{-1})	HR (%)	RMSE (m s^{-1})
BLM	73	3.0	64	3.7	54	3.7	64	3.4	62	3.3
Eta	21	5.6	18	6.8	15	6.5	18	6.4		

Table 4 presents the results of Experiment III and shows, as in the two previous experiments, forecast degradation with time. Figure 4 shows that the BLM HR at every weather station is, on average, better than that of the Eta forecasts. When comparing the results of Experiment III with the other two experiments, the HR is always equal or better at every weather station, except at Colonia. For comparison, the BLM is run with the upper boundary condition taken from the 1,000-hPa Eta forecasts (Table 3, column 2), but in this case the results worsen since the HR decreases from 59 to 53%, although the RMSE remains unchanged at 3.4 m s^{-1}.

Table 5 compares the results of the three experiments by time of day. Experiment III is the most accurate, on average (rightmost two columns), as well as at 0900 LST and 1500 LST. However, at 2100 LST Experiment I results are more accurate, indicating that the use of forecast boundary conditions is better than persistence, for longer lead times. Also, in all cases the BLM wind forecasts are more accurate than the Eta forecasts, since the BLM RMSE is between 1.9 and 3.3 m s^{-1} smaller than the Eta RMSE, and the HR is more than three times greater than that of the Eta forecasts. Table 5 also shows systematic forecast degradation with time in Experiment III, which uses only observations for the boundary conditions. On the other hand, when the boundary conditions are exclusively defined from the Eta forecasts, as in Experiment I, the 12-h (2100 LST) forecast is not only more accurate than the 6-h forecast, but also unmatched. These results indicate, for longer lead forecasts, the clear advantage of using the Eta model predictions for defining the BLM model boundary conditions.

Table 5 Averaged HR and RMSE values for each BLM model experiment and the Eta model

	0900 LST		1500 LST		2100 LST		Average 0900, 1500 and 2100 LST		Average from 0900 to 2100 LST	
	HR (%)	RMSE ($m\ s^{-1}$)	HR (%)	RMSE ($m\ s^{-1}$)	HR (%)	RMSE ($m\ s^{-1}$)	HR (%)	RMSE ($m\ s^{-1}$)	HR (%)	RMSE ($m\ s^{-1}$)
BLM Exp I	68	3.2	50	3.5	58	3.6	59	3.4	58	3.5
BLM Exp II	64	3.7	60	4.2	45	3.7	56	3.8	58	4.3
BLM Exp III	73	3.0	64	3.7	54	3.7	64	3.4	62	3.3
Eta	21	5.6	18	6.8	15	6.5	18	6.4		

3.5 Example of Forecast for 18 January 2004

Since point verification may not be well suited for quantifying forecast models, and only standard meteorological observations are available in the region, a qualitative measure of verification is implemented. The BLM vertical velocity forecast is compared to the cumulus cloud distribution of a satellite image, in order to give a regional scale assessment of the model ability. As an example, this section presents the forecast for 18 January 2004, a date that was chosen with the following consideration. A first screening identified the days with an 850-hPa Eta forecast of light winds from the east or north-east throughout the daytime hours. This is the appropriate regional condition for the development of the typical low clouds that are induced by the sea-breeze circulation in the region. Out of the initially identified 7 days, the date of the example was the only one with a clear satellite image available around noon.

Firstly, the 10-m wind field forecasts of the BLM and Eta models are compared to the observations. Figure 5a shows the BLM forecast at 0900 LST along with the wind observations (thick arrows) at the five weather stations of the study (left panel), and the Eta forecast (right panel). The wind field for both models is mainly from the east and north-east, in agreement with the observations. However, there are discrepancies in the wind speeds since the Eta forecast around the weather stations in Argentina shows smaller values than the BLM forecast, which in turn agrees better with the observations. Besides, the BLM winds are weaker over the river and stronger over the land, whereas the Eta forecast shows systematically decreasing wind speeds from east to west.

Figure 5b corresponds to 1500 LST, the time of the day when the sea breeze is well developed. The Eta forecast shows south-easterly winds across the river and neighbouring regions, whereas the observations reveal different wind directions. Over the coastal region of Uruguay the BLM and the Eta wind direction forecasts are from the south-east, in agreement with the observations. Over the coastal region of Argentina the BLM wind direction forecast is east, which agrees with the observations, whereas the Eta wind direction forecast is south-east. The observed wind pattern over the region of the river springs displays the inland sea-breeze component, which is very well represented by the BLM forecast but clearly ignored by the Eta forecast.

Figure 5c corresponds to 2100 LST, when the observed wind direction field over the coast of Uruguay does not show changes with respect to the 1500 LST forecast. The BLM wind direction forecast agrees with the observations, whereas the Eta forecast shows a wind direction shift to the eastern sector over the entire northern half of the region. Over the coast of Argentina the BLM forecast shows easterly and east-south-easterly winds, mostly in

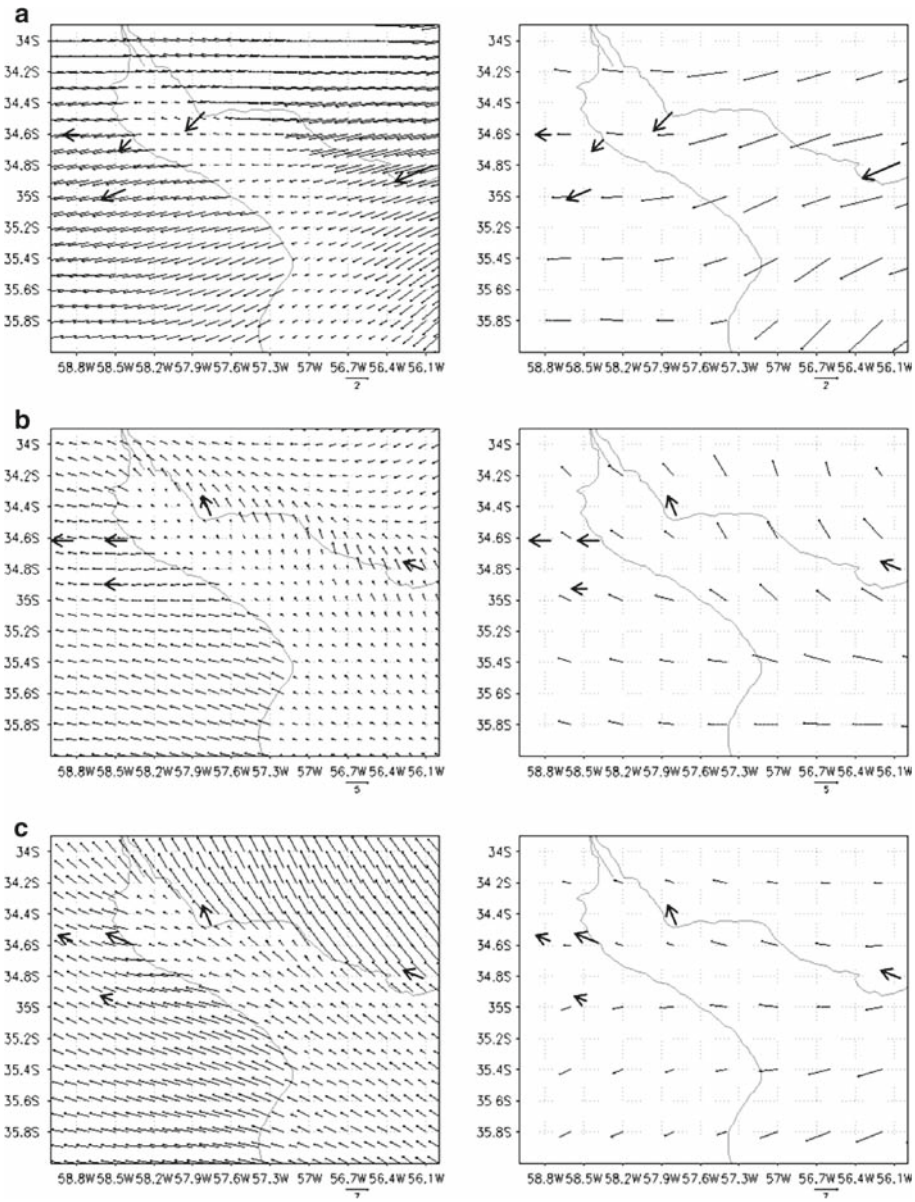

Fig. 5 Example of 10-m wind field forecast of the BLM model (*left panels*) and the Eta model (*right panels*). The *bold arrows* represent the standard wind observations at the five weather stations. The date is 18 January 2004 and panel **a** corresponds to 0900 LST, panel **b** corresponds to 1500 LST and panel **c** corresponds to 2100 LST

agreement with the observations. Instead, the counter-clockwise wind direction change from panel (b) to (c) of the Eta forecast is opposed to the observed one, between 1500 LST and 2100 LST.

The comparison of the wind fields at these three times clearly reveals the significant variability in time and space of the sea–land breeze circulation across the region. On the other

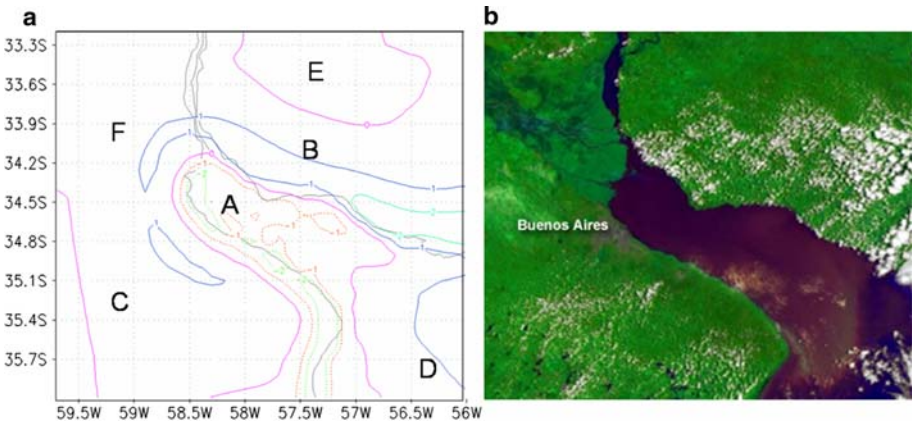

Fig. 6 **a** BLM vertical velocity forecast at 1,200 m corresponding to 1100 LST of 18 January 2004; **b** NOAA-17 satellite image at 1344 UTC (1044 LST) provided by the National Meteorological Service of Argentina

hand, these changes are reasonably well represented by the BLM forecast, particularly over the river springs, but completely ignored by the Eta forecast.

Figure 6a presents the forecast vertical velocity field at 1,200 m for 1100 LST, 18 January 2004. The regions identified with letters A and E display downward motion, whereas the rest of the domain displays upward motion. Since there are no vertical velocity observations available, it is possible to perform a qualitative verification of the vertical motion by analyzing the cumulus cloud distribution of a satellite image. Figure 6b shows the 1344 UTC (1044 LST) NOAA-17 satellite image, in which the low-level cumulus clouds can be clearly identified. The region identified with letter A in Fig. 6a matches the cloud free region over most of the river and the neighbouring inland region of Argentina of Fig. 6b. The region identified with letter B in Fig. 6a displays upward motion over land and up to the river shore, in coincidence with the cumulus cloud distribution in Fig. 6b, whereas in region C the clouds are located further inland (Fig. 6b); in agreement with the vertical motion field of Fig. 6a. Over the river mouth (Fig. 6b) there are scattered clouds, again in agreement with the upward motion of region D in Fig. 6a. Region E (Fig. 6a), inland over Uruguay and far from the river, is characterized by downward motion, coinciding with a cloud free region in Fig. 6b. Region F is clearly the one without any qualitative agreement between cloudiness and vertical motion. There, the model results indicate upward motion, with a maximum near the coast, whereas the satellite image is free of clouds. One of the tributaries of the La Plata River is the Uruguay River, which can be clearly seen in the satellite image coming from the north. The other tributary is the Paraná River, which drains from the north-west (upper left corner of Fig. 6b), and despite having flow that double the flow of the Uruguay River, is not clearly visible in the image. This is because the Paraná River runs along multiple streams that form a river delta, merging the La Plata River immediately to the north-west of the city of Buenos Aires. Therefore, a significant part of region F is a very humid flatland where the river–land temperature contrast is not confined to a narrow region as in the rest of the La Plata River shores. This singularity modifies the convergence/divergence pattern of the horizontal motion and, consequently, the vertical motion as well. Since the BLM model does not consider different soil types, this particular characteristic of region F is not represented, which in turn may explain the disagreement between the observed cloud distribution and the predicted vertical motion.

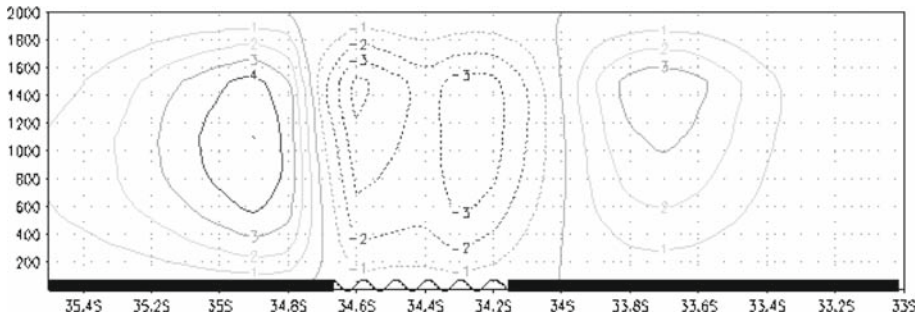

Fig. 7 Vertical cross-section at 58.8°W of the BLM vertical velocity forecast at 1500 LST

Figure 7 presents a vertical cross-section at 58.4°W of the BLM vertical velocity forecast for 1500 LST. At this time of the day the sea breeze is at its peak, so that the land regions display upward motion and the river region, at the centre of the figure, displays downward motion. This vertical velocity pattern is typical of a well-developed mid-afternoon sea-breeze circulation that results from the low-level wind convergence/divergence fields. A similar vertical cross-section of the Eta forecast (not shown) does not reveal any detail since the magnitude of the vertical motion is of the order of 0.1 mm s^{-1}, with no clearly defined spatial pattern.

4 Discussion and Conclusions

A mesoscale boundary-layer model (BLM) is used for forecasting the low-level wind field over the La Plata River region during the period November 2003–April 2004. Three experiments are performed in which the BLM is forced with the Eta/CPTEC model forecasts (Experiment I), with local observations (Experiment III), as well as a combination of observations and forecasts (Experiment II). The quality of forecasts is evaluated by comparing the 10-m observed wind at five weather stations in the region, with the forecast wind averaged over the four grid points that surround each weather station. Two error measures are employed: one is the percentage of cases with agreement in the 8–sector wind direction, i.e. the hit rate (HR), and the other is the root-mean-squared error (RMSE) of the horizontal wind components. As an additional and qualitative measure of verification, the vertical velocity field forecast by the model is compared to the cumulus cloud distribution of a satellite image.

In Experiment I the BLM is forced with the Eta 850-hPa wind forecasts at the upper boundary and the Eta surface temperature forecasts at the lower boundary. The BLM wind forecasts are substantially better than the Eta wind forecasts. The BLM RMSE is about 50% smaller, and the HR is more than three times greater, than the corresponding Eta forecasts. The river–land temperature differences forecast by the Eta model are always greater than the observed ones, the consequence of which is a degradation of the wind direction forecast, since the excessive thermal forcing creates a stronger than normal inland wind component during the afternoon. In view of this problem, Experiment II defines the surface forcing as a function of the observed temperature difference between Ezeiza (land) and Pontón Recalada (river) weather stations. The wind direction forecast is significantly better in the afternoon, although it is accompanied by a small degradation of the wind-speed forecast. On the other hand, the degradation of the wind direction forecast by the evening is larger than in

Experiment I, indicating that the forecast improvement achieved during the first hours cannot be sustained with time.

Experiment III is designed to validate the BLM forecasts when forced exclusively with observations. The lower boundary condition is the same as in Experiment II, while the upper boundary condition is taken from the 0900 LST Ezeiza radiosonde sounding at the three standard levels within the boundary layer, i.e. 850, 925 and 1,000 hPa. When the 850 and 925 hPa levels are used, the forecast results are not better than those of Experiment I. Instead, the 1,000-hPa level provides the best result since the error measures are the minimum of all experiments. The South Atlantic anticyclone has a strong influence over the La Plata River region and its temperature inversion defines the top of the boundary layer. The morning sounding reveals that most of the time the temperature inversion is below 925 hPa, and this may be the reason why the best result is obtained when forcing the model at the upper boundary condition with the 1,000-hPa data.

The BLM forecasts show greater degradation with time when the boundary conditions are defined exclusively from the observations. On the other hand, when they are defined exclusively from the Eta forecasts, the 12-h forecasts are more accurate than the 6-h forecasts. This result clearly indicates the advantage of using the Eta model outputs for defining the boundary conditions for longer lead BLM forecasts.

Although the short lead forecasts improve when forcing the BLM with observations, this case has operational disadvantages. Since the model is forced with the only daily radiosonde sounding at 0900 LST, the synoptic scale changes that may take place during the forecast period are ignored. Also, the necessity of specifying the lower boundary forcing as a function of time would require a forecast of the land–river temperature difference, so that an additional uncertainty may affect the final result. In any case this method would allow for a 12-h forecast for the rest of the day, but, on the other hand, the use of 48-h Eta model outputs for forcing the BLM allows for a forecast with 1 day in advance, i.e. 36-h lead forecast.

As an additional measure of verification, the vertical velocity field forecast by the model is compared to the cumulus cloud distribution of a satellite image, in order to have a regional scale assessment of the model simulation. The result shows a good agreement between the spatial patterns in most parts of the region, i.e. cumulus cloud areas (cloud free areas) coincide with the areas where the model predicts upward (downward) motion.

The improvement of the low-level wind forecast obtained with the BLM model, in comparison to the Eta model forecast, is not a straightforward consequence of the higher horizontal resolution of the former, in terms of grid spacing. An additional experiment is performed in which the BLM is forced at the lower boundary with the Eta model surface temperature forecasts, with the following consideration. The Eta model outputs are simply interpolated to the BLM resolution, i.e. ignoring the coastal geometry as in all other experiments. The result, although representing a minor improvement over the Eta forecasts, is far from achieving the performance of Experiment I. It is clear that the advantage of using the BLM model for forecasting the low-level wind field over the La Plata River region is the result of a more appropriate definition of the land–river surface temperature contrast. The particular formulation that the BLM model has for the geometry of the river coasts is fundamental for resolving the smaller scale details of the low-level local circulation.

Despite the large errors in the surface winds displayed by the Eta forecasts, its 850-hPa wind and surface temperature forecasts are able to drive the BLM model to obtain surface wind forecasts with smaller errors than the Eta model. Thus, the main conclusion of the study is that operational low-level wind forecasts for the La Plata River region can be improved by forcing the BLM model with the Eta operational forecasts.

Acknowledgments This research was partially supported by research grants PIP5575 from Consejo Nacional de Investigaciones Científicas y Técnicas (CONICET) of Argentina, UBACYT X835 from Universidad de Buenos Aires and PICT2005-38193 from Agencia Nacional de Promoción Científica y Tecnológica of Argentina. The authors are grateful to Marcelo Seluchi from CPTEC for providing the Eta model forecasts, and to Diana Rodriguez from the National Meteorological Service of Argentina for preparing the satellite image. L. Sraibman acknowledges CONICET for granting a doctoral fellowship. The article is based on L. Sraibman's Ph.D. thesis at the University of Buenos Aires.

References

Berri GJ, Nuñez MN (1993) Transformed shoreline-following horizontal coordinates in a mesoescale model: a sea–land breeze case study. J Appl Meteorol 5:918–928

Black TL (1994) The new NMC mesoscale Eta model: description and forecast examples. Weather Forecast 9:265–278

Bustamante J, Gomes JL, Chou SC, Rozante JR (1999) Evaluation of April 1999 rainfall forecasts over South America using the Eta Model. Climanálise, No. 5, Cachoeira Paulista, SP, Brazil

Case JL, Manobianco J, Lane JE, Immer CD, Merceret FJ (2004) An objective technique for verifying sea breezes in high-resolution numerical weather prediction models. Weather Forecast 19:690–705

Colby FP Jr (2004) Simulation of the New England sea breeze: the effect of grid spacing. Weather Forecast 19:277–285

Cormier DR, Marsh L (2001) Spline regression models. Sage Publications, Thousand Oaks, 80 pp

Cressman GP (1959) An operative objective analysis scheme. Mon Wea Rev 87:367–374

Daggupaty SM (2001) A case study of the simultaneous development of multiple lake-breeze fronts with a boundary layer forecast model. J Appl Meteorol 40:289–311

Hanna SR, Yang R (2001) Evaluations of mesoscale models' simulations of near-surface winds, temperature gradients, and mixing depths. J Appl Meteorol 40:1095–1104

Mesinger F, Black TL (1992) On the impact on forecast accuracy of the step-mountain (eta) vs. sigma coordinate. Meteorol Atmos Phys 50:47–60

Pielke RA (1974) A three dimensional numerical model of the sea breezes over the South Florida. Mon Wea Rev 102:115–139

Pielke RA, Cotton WR, Walko RL, Tremback CJ, Lyons WA, Grasso LD, Nicholls ME, Moran MD, Wesley DA, Lee TJ, Copeland JH (1992) A comprehensive meteorological modeling system RAMS. Meteorol Atmos Phys 49:69–91

Roebber PJ, Gehring MG (2000) Real-time prediction of the lake breeze on the western shore of Lake Michigan. Weather Forecast 15: 298–312

Seluchi ME, Chou SC (2001) Evaluation of two Eta model versions over South America. Rev Geofis 40:219–238

White BG, Paegle J, Steenburgh JW, Horel JD, Swanson RT, Cook LK, Onton DJ, Miles JG (1999) Short-term forecast validation of six models. Weather Forecast 14:84–108

Wilks DS (1995) Statistical methods in the atmospheric sciences. Academic Press, New York, 240 pp

Zhang Y, Chen Y, Schroeder TH, Kodama K (2005) Numerical simulations of sea-breeze circulations over northwest Hawaii. Weather Forecast 20:827–846

Zhong S, Fast J (2003) An evaluation of the MM5, RAMS, and Meso-Eta models at subkilometer resolution using VTMX field campaign data in the Salt Lake Valley. Mon Wea Rev 131:1301–1322